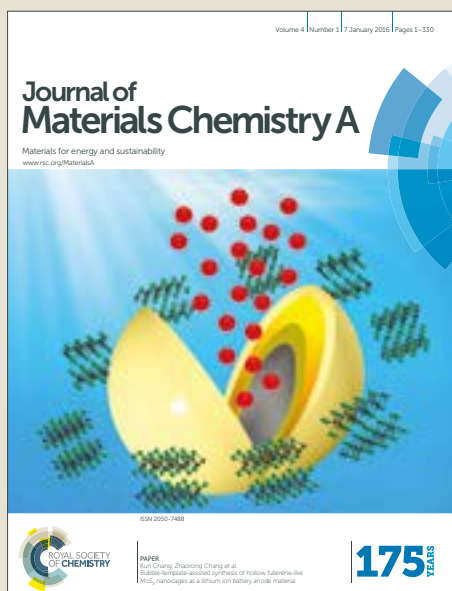


Journal of Materials Chemistry A

Accepted Manuscript



This article can be cited before page numbers have been issued, to do this please use: C. Li, F. Wu, C. Liang, K. Ho and J. T. Lin, *J. Mater. Chem. A*, 2017, DOI: 10.1039/C6TA11091F.



This is an Accepted Manuscript, which has been through the Royal Society of Chemistry peer review process and has been accepted for publication.

Accepted Manuscripts are published online shortly after acceptance, before technical editing, formatting and proof reading. Using this free service, authors can make their results available to the community, in citable form, before we publish the edited article. We will replace this Accepted Manuscript with the edited and formatted Advance Article as soon as it is available.

You can find more information about Accepted Manuscripts in the [author guidelines](#).

Please note that technical editing may introduce minor changes to the text and/or graphics, which may alter content. The journal's standard [Terms & Conditions](#) and the ethical guidelines, outlined in our [author and reviewer resource centre](#), still apply. In no event shall the Royal Society of Chemistry be held responsible for any errors or omissions in this Accepted Manuscript or any consequences arising from the use of any information it contains.



Journal Name

ARTICLE

Effective Suppression of Interfacial Charge Recombination by 12-Crown-4 Substituent on Double-Anchored Organic Sensitizer and Rotating Disk Electrochemical Evidence

Chun-Ting Li,^a Feng-Ling Wu,^a Chia-Jung Liang,^a Kuo-Chuan Ho,^b and Jiann T. Lin^{a,*}

Received 00th January 20xx,
Accepted 00th January 20xx

DOI: 10.1039/x0xx00000x

www.rsc.org/

Mono/double-anchored phenothiazine-based dyes (**DCE1–DCE4**) containing various *N*-substituents (12-crown-4-substituted phenyl, 4-hexoxyphenyl, and bare phenyl) have been synthesized and applied as the sensitizers for dye-sensitized solar cells (DSSCs). 12-Crown-4-substituted phenyl entity on the double-anchored dye effectively retards the dark current via Li⁺ chelation in the case of LiI redox mediator or steric blockade of Co-phen³⁺ in the case of cobalt redox mediator. The retarded dark current was further confirmed from the recombination rate constant for the reduction of the oxidized redox mediators at the photoanode/electrolyte interface by rotating disk electrode technique. The **DCE2**-based DSSC with iodide-based electrolyte exhibited a good cell efficiency up to 8.82%, which surpassed that of the N719-based DSSC (8.20%). With cobalt-based electrolyte, higher cell efficiencies of 10.12% and 11.17% were obtained at 1 sun and 0.1 sun, respectively, using a Pt-free and TCO-free counter electrode.

1. Introduction

Dye-sensitized solar cells play an important role in the development of the third generation solar cells, including Miyasaka's pioneer work on perovskite solar cell,¹ which later evolved into high performance mesoscopic perovskite solar cells.^{2–4} As a heart material in dye-sensitized solar cells (DSSCs), plenty types of dyes were developed, *e.g.*, ruthenium dyes (CYC-B11, 11.5%),⁵ zinc dyes (SM315, 13.0%),⁶ and metal-free organic dyes (C281, 13.0%;⁷ the co-sensitization of ADEKA-1 and LEG4, 14.3%).⁸ Among them, metal-free organic dyes stood out due to their flexibility in molecular design, high molar extinction coefficients, and high efficiency. In a DSSC, the major energy loss occurs at the photoanode/electrolyte interface due to the recombination reactions of the photo-induced electrons at the TiO₂ surface with two kinds of materials, *i.e.*, the oxidized dye and the oxidized redox mediators.^{9, 10} The recombination reaction with the oxidized mediator will cause the dark current, decrease the electron density as well as the Fermi level of TiO₂, and thus lead to a lower open-circuit voltage (*V*_{OC}) of the DSSC, as the *V*_{OC} value is determined by the potential difference between the Fermi level of TiO₂ and the redox potential of the mediator. To tackle

the dark current, two approaches are frequently used: (i) grafting alkyl/bulky groups at the donor moiety or the π bridge of metal-free dyes^{11–14} and (ii) having appropriate amount of anchors (double or multi-anchors).^{15–17} Therefore, the oxidized redox mediator can be effectively blocked or the TiO₂ surface can be effectively protected.

We recently found that phenothiazine-based dyes with double anchors (D($-\pi$ -A)₂) not only more efficiently suppressed the dark current, but also provided more electron extraction pathways, compared to their congeners with mono-anchor.^{18–20} Besides, the *N*-substituent of the phenothiazine entity offered the opportunity for alleviation of dark current as well as dye aggregation; the pertinent DSSCs thus reached higher cell efficiency than the N719-based standard cell. Adsorption of lithium cation (Li⁺), frequently used counter-ion of the iodide or the supporting electrolyte for the cobalt redox mediator, was known to enhance dark current.^{21–23} Prevention of Li⁺ from its electrostatic interaction with the photo-induced electrons on the TiO₂ surface was deemed a promising approach to suppress dark current.^{24, 25} In previous researches, the incorporation of oligo(ether)-based segment in dye molecular helped with chelating Li⁺ and quarantining I₃⁻ from the TiO₂ surface.^{26–29} In addition, the fettered I⁻ ion by the Li⁺ close to the regenerating site of the dye may benefit dye regeneration. Crown ethers have high affinity for alkali metal ions via the lone pair electrons at the oxygen atoms,^{30–32} and 12-crown-4 is particularly suitable for Li⁺ binding due to its specific size of cavity.^{33, 34} White *et al.*³⁵ and Uemura *et al.*³⁶ synthesized the crown ether-substituted ruthenium dye (RC730, 1.87%) and carbazole dye (MK-70, 5.50%), respectively.

^a Institute of Chemistry, Academia Sinica, No. 128, Sec. 2, Academia Road, Nankang District, Taipei 11529, Taiwan

^b Department of Chemical Engineering, National Taiwan University, No. 1, Sec. 4, Roosevelt Road, Taipei 10617, Taiwan

Electronic Supplementary Information (ESI) available: [details of any supplementary information available should be included here]. See DOI: 10.1039/x0xx00000x

ARTICLE

Journal Name

However, these crown ether-substituted dyes gave cell efficiencies similar to those of their analogues without the crown ether entity. The role of crown ether in those dyes toward the DSSCs' performance is still blurry up-to-date. Our earlier success of using oligo(ether) substituent in phenothiazine-based mono-anchored dyes for the DSSCs with high photovoltage and high efficiency²⁶ prompted us to explore the possibility of double-anchored phenothiazine dye with a 12-crown-4 substituent at the nitrogen atom of phenothiazine entity. Herein we report new sensitizers of the type and their highly efficient DSSCs. The role of the crown is also elucidated via different physical studies including rotation disk electrode electrochemical measurements.

2. Results and discussion

2.1. Synthesis of DCE dyes

The synthetic routes for new DCE dyes are depicted in Scheme 1. Figure 1 shows that DCE1 is a mono-anchored dye and DCE2–DCE4 are double-anchored dyes with different *N*-substituents at their phenothiazine entities (including 12-crown-4-substituted phenyl, 4-hexoxyphenyl, and bare phenyl substituents). At first (step i), the 12-crown-4-substituted phenyl (or 4-hexoxyphenyl, or bare phenyl entity) was introduced at the nitrogen atom of the phenothiazine core through Pd(dba)₂ (dba = dibenzylideneacetone)-catalyzed C–N coupling reaction^{37, 38} with 10*H*-phenothiazine. The key intermediate, **5**, of the mono-anchored DCE1 dye is prepared

from **1** through a Vilsmeier–Haack reaction (step ii) followed by a bromination reaction (step iii), where these steps are referred to the reported procedures.²⁶ Subsequently, a triethyleneoxide methyl ether (TEOME)-substituted phenyl entity is attached to the molecule through the C-3 (or C-7) position of the phenothiazine by a palladium-catalyzed Suzuki–Miyaura C–C coupling reaction³⁹ between TEOME-substituted phenyl bromide and dioxaborolyl phenothiazine (step v). Lastly, the desired product, DCE1, is obtained via Knoevenagel condensation of the appropriate aldehyde (DCE1a) with cyanoacetic acid (step vi).

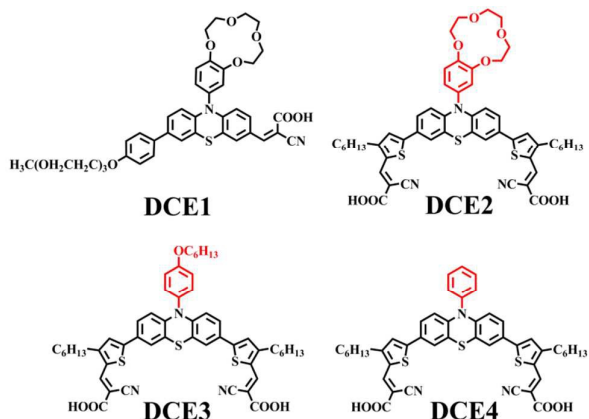
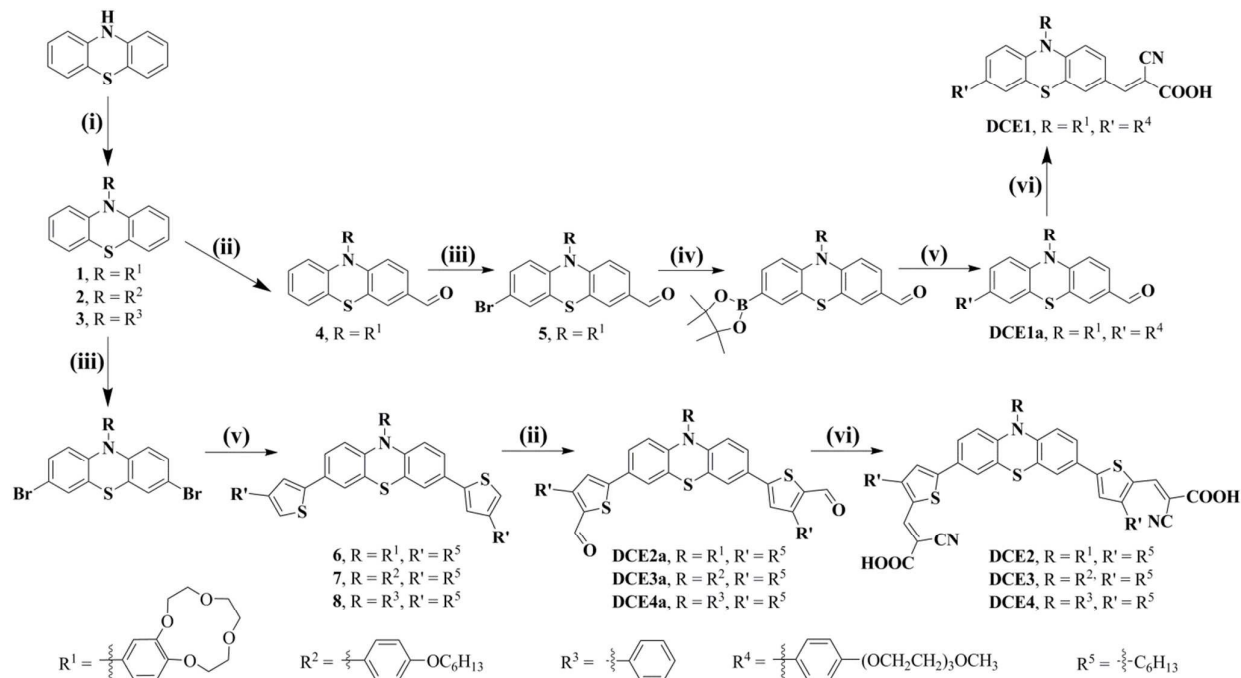


Figure 1. Molecular structures of the DCE dyes.



Scheme 1. Synthetic route of the DCE dyes. (i) 10*H*-phenothiazine, Pd(dba)₂ (where dba = dibenzylideneacetone), Pt(Bu)₃, NaOtBu, toluene, 120 °C, 20 h; (ii) POCl₃, DMF, 60 °C, 18 h; (iii) *N*-bromosuccinimide (NBS), CH₂Cl₂, 18 h; (iv) bis(pinacolato)diboron, KOAc, PdCl₂(dppf) (where dppf = 1,1'-bis(diphenylphosphino)ferrocene), 1,4-dioxane, 120 °C, 20 h; (v) Pd(PPh₃)₄, 2M K₂CO₃, 1-bromo-2,4-bis[2-(2-methoxyethoxy)ethoxy]ethoxy]benzene, toluene, 120 °C, 20 h; (vi) cyanoacetic acid, NH₄OAc, AcOH, 120 °C.

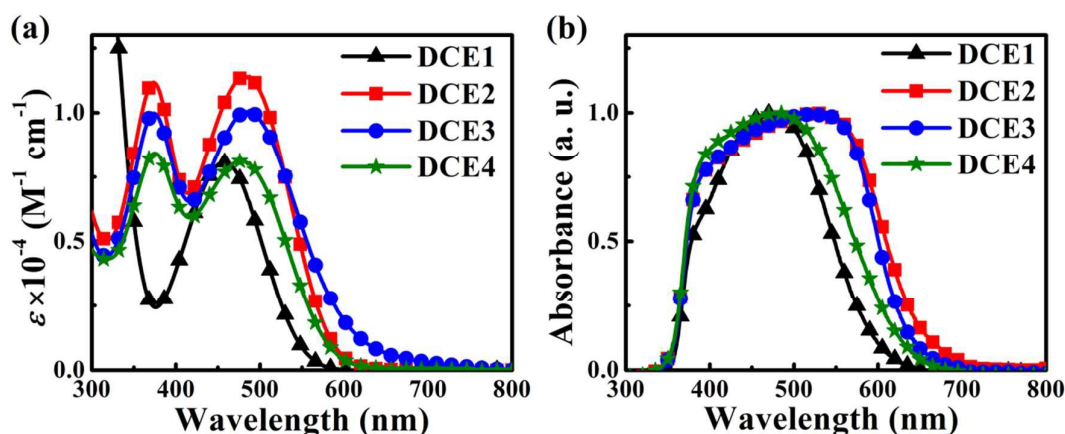


Figure 2. Absorption spectra of DCE dyes (a) dissolved in THF (10 mM) and (b) adsorbed on TiO₂ film (4 μm).

To synthesize the double-anchored dyes, the key intermediates, **6**, **7**, and **8**, are prepared from **1**, **2**, and **3**, respectively; through a bromination reaction (step iii) followed by a Suzuki–Miyaura C–C coupling reaction between the dibromo phenothiazine and the appropriate thiophene dioxaborolanes (step v). Finally, the desired products, **DCE2** to **DCE4**, are obtained via the Vilsmeier–Haack reaction (step ii) followed by a Knoevenagel condensation reaction.^{18–20, 40} Detailed synthetic information for the **DCE** dyes are depicted in the Supporting Information.

2.2. Optical properties and DFT calculations of DCE dyes

The double-anchored dyes (**DCE2**–**DCE4**) have the intramolecular charge-transfer transition (ICT) band absorption peak ($\lambda_{\text{abs}}^{\text{THF}}$) at the wavelength of 477 to 488 nm, which is about 20–30 nm larger than that of **DCE1** (Figure 2a and Table 1). This can be attributed to the extension of π -conjugation length in the double-anchored dyes.¹⁸ Accordingly, the optical HOMO/LUMO gaps ($E_{\text{g}}^{\text{opt}}$) for double- and mono-anchored dyes are about 2.1–2.2 eV and 2.42 eV, respectively. The double-anchored dye with an electron-donating substituent (*i.e.*, **DCE2** or **DCE3**) exhibits only slightly larger $\lambda_{\text{abs}}^{\text{THF}}$ and molar extinction coefficient (ϵ) than its congener with a bare phenyl substituent (**DCE4**), owing to the large twist angle

between the phenothiazine and the *N*-phenyl substituent (*vide infra*). Red shift of the ICT band for the **DCE** dyes-adsorbed TiO₂ films (Figure 2b) and tailing of the absorption band edges ($\lambda_{\text{onset}}^{\text{film}}$) beyond 650 nm reflect *J*-aggregation of the dyes on the TiO₂ films.

Comparable oxidation potentials (E_{ox}) of the dyes measured by cyclic voltammograms (Figure S1) indicate that the variation of the *N*-substituent of phenothiazine barely influences the HOMO level of the dye. This result is substantiated by density functional theory (DFT) and time-dependent DFT (TDDFT) calculations. Selected frontier orbitals and low-lying transitions are shown in Figure S2 and Table S1, respectively. All dyes exhibit comparable HOMO level suitable for dye regeneration and appropriate LUMO level for electron injection (Figure S3). Nearly 100% $S_0 \rightarrow S_1$ (HOMO \rightarrow LUMO) transition in all dyes (Table S1) indicates prominent charge transfer from the phenothiazine donor to the anchor. Broader ICT band in double-anchored dyes than in **DCE1** is attributed to the mixing of $S_0 \rightarrow S_1$ with low energy $S_0 \rightarrow S_2$ transitions. Both anchors on the double-anchored dyes can function as electron injection channels based on the following observations: (1) they both contribute to the LUMO orbital (Figure S3), and (2) they both possess significant negative charges at the excited state, as shown in the Mulliken charge plots (Figure S4).

Table 1. Optical and electrochemical data of the dyes, and their photovoltaic parameters for iodide-based DSSCs

Dye	Optical and electrochemical properties ^[a]					Photovoltaic properties ^[f]				
	$\lambda_{\text{abs}}^{\text{THF}}$ [nm] ($\epsilon \times 10^{-4} \text{ M}^{-1} \text{ cm}^{-1}$)	$E_{\text{g}}^{\text{opt}}$ [eV] ^[b]	$\lambda_{\text{onset}}^{\text{film}}$ [nm] ^[c]	E_{ox} [V] ^[d]	E_{0-0}^* [V] ^[e]	V_{oc} [mV]	J_{sc} [mA cm ⁻²]	<i>FF</i>	η [%]	Dye loading [mol cm ⁻²]
DCE1	457 (0.80)	2.42	650	1.08	-1.34	658.8±1.41	11.95±0.10	0.69±0.00	5.44±0.04	3.94×10 ⁻⁷
DCE2	487 (1.14)	2.15	730	1.06	-1.09	706.0±2.44	18.19±0.03	0.69±0.00	8.82±0.01	2.38×10 ⁻⁷
DCE3	488 (1.01)	2.09	700	1.09	-1.00	680.1±2.34	18.16±0.04	0.65±0.00	7.99±0.01	2.26×10 ⁻⁷
DCE4	477 (0.82)	2.16	675	1.07	-1.09	666.5±1.41	15.64±0.20	0.67±0.00	7.02±0.10	2.88×10 ⁻⁷

^[a]Based on THF solution at 298 K. ^[b]Calculated via $E_{\text{g}}^{\text{opt}} = 1240/\lambda_{0-0}$, where λ_{0-0} is read from the cross point of absorption and emission spectra. ^[c]Based on 4 μm-thick TiO₂ film. ^[d]Adjusted to be versus to normal hydrogen electrode (NHE) using ferrocene/ferrocenium as an internal reference. ^[e]Calculated via $E_{0-0}^* = E_{\text{ox}} - E_{\text{g}}^{\text{opt}}$ (vs. NHE).

^[f]Measured at AM 1.5G based on five DSSCs with I⁻/I₃⁻ electrolyte.

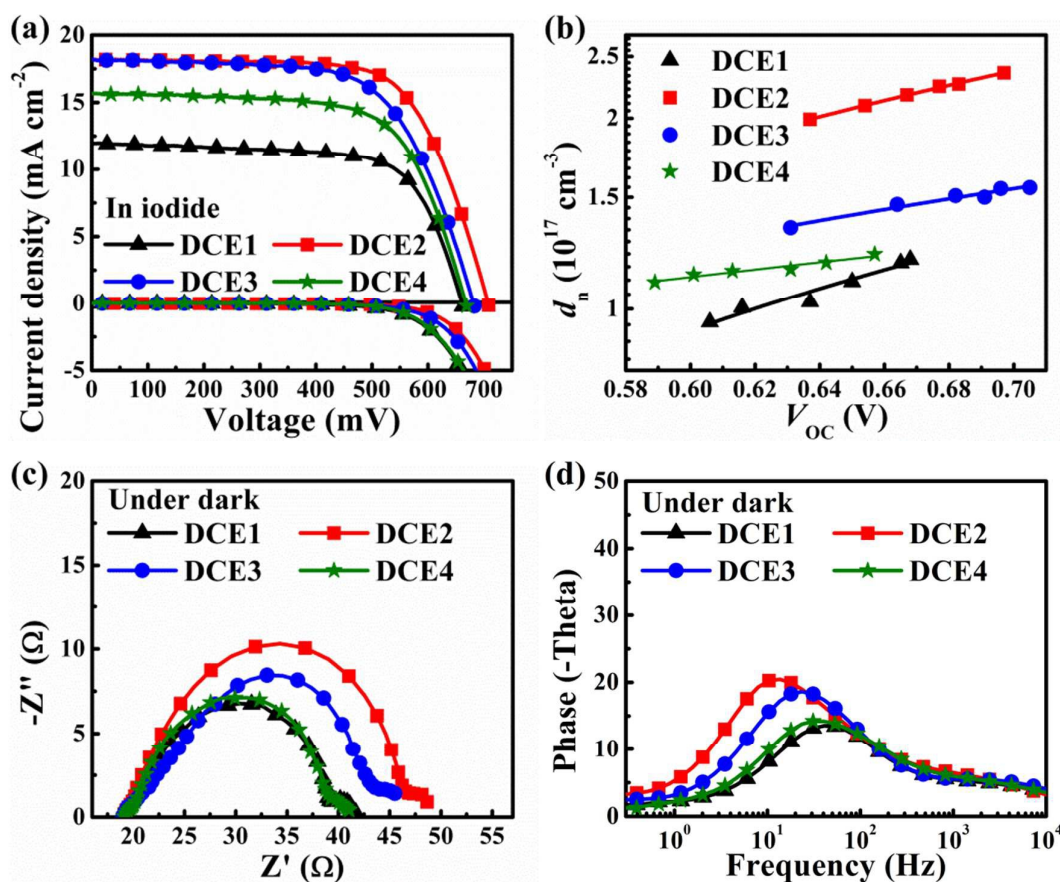


Figure 3. Plots of photovoltaic performance for the DSSCs with various DCE dyes using Γ^-/I_3^- redox mediator: (a) the current density–voltage curves, measured under simulated AM 1.5G illumination or dark condition, (b) the extracted electron density–photovoltage curves, measured under an intensity-modulated (10 to 300 W m^{-2}) white-light-emitting diode, (c) and (d) the electrochemical impedance spectra (Nyquist and Bode plots, respectively), measured under dark at an applied bias of -0.70V .

The dihedral angle between the phenothiazine and the *N*-substituted phenyl ring falls in the range from 82.6° to 83.9° (Figure S5), which may result in minute electronic communication between these two entities. Consequently, the ICT bands of DCE2–DCE4 have similar absorption maxima and intensity.

2.3. Photovoltaic performance of the cells with various DCE dyes

Photocurrent density–voltage curves (Figure 3a) of the DSSCs coupled with various DCE dyes were measured under simulated AM 1.5G illumination using Γ^-/I_3^- redox mediator. In Table 1, all double-anchored dyes (DCE2–DCE4) have higher cell efficiencies (η : 7.31–8.41%) than the mono-anchored DCE1 (6.31%), owing to the higher open-circuit voltage (V_{oc}) and short-circuit current density (J_{sc}). Although DCE1 possesses the largest dye-loading amount on TiO_2 thin film, the most blue-shifted spectral range and lowest absorptivity result in the least J_{sc} value of its DSSC. The smaller J_{sc} for DCE4 than DCE2 and DCE3 is also attributed to the narrower and weaker absorption for DCE4 (both in solution and on the TiO_2 film). The V_{oc} values for DCE dyes decrease in the order of DCE2 (706 mV) > DCE3 (680 mV) > DCE4 (667 mV) \approx DCE1 (658 mV).

The V_{oc} value of a DSSC is influenced by the conduction band edge (E_{CB}) of the dye-adsorbed TiO_2 film and the retardation ability of the dye against dark current.^{22, 23} Via charge-extraction technique, the electron density (d_n) on the DCE dye-adsorbed TiO_2 film decreases in an order of DCE2 > DCE3 > DCE4 > DCE1 (Figure 3b), indicating that all double-anchored DCE dyes exhibit a downward shift of the E_{CB} of TiO_2 film compared with mono-anchored DCE1.^{41, 42} The outcome is attributed to the release of two protons from the double-anchored dye upon dye adsorption on the TiO_2 surface.^{18, 43} Therefore, the higher V_{oc} values for the double-anchored DCE dyes imply that the dark current suppression efficiency predominates over the E_{CB} shift in these cells. This is consistent with previous findings that double-anchored dyes are more effective in suppressing the dark current (vide infra).¹⁸ It is commonly found that efficient dark current suppression leads to higher V_{oc} value of the cells.^{7, 14, 44, 45} Among the three substituents in double-anchored DCE dyes, 12-crown-4-substituted phenyl moiety is the most sterically congested, and phenyl moiety is the least, suggesting that steric factor plays an important role in suppressing the dark current. We previously also found that more sterically hindered *N*-substituent in double-anchored phenothiazine dyes could

suppress the dark current more effectively:⁴⁰ bis(2-ethylhexyloxy)phenyl moiety (750 mV) > bis(*n*-hexyloxy)phenyl moiety (730 mV) > 2-ethylhexyl moiety (680 mV).

Moreover, **DCE2** has high affinity toward Li⁺ via its 12-crown-4-substituted phenyl moiety, preserving the E_{CB} of TiO₂ in addition to the retardation of charge recombination,^{33, 34, 42, 46} thus, **DCE2** gives the highest V_{OC} . The V_{OC} value as well as the retardation ability against the dark current for the mono-anchored **DCE1** is the least among all **DCE** dyes, even though **DCE1** has the most favorable E_{CB} of TiO₂ and the beneficial 12-crown-4 entity. This most probably stems from more severe dye aggregation of **DCE1**, as evidenced from the clear blue-shift in its incident photon-to-current conversion efficiency (IPCE, **Figure S6a**) spectra after using chenodeoxycholic acid (CDCA) as the co-adsorbent. The argument on the correlation of V_{OC} value with dark current suppression is verified via the dark current density–voltage curves shown in the lower part of **Figure 3a**. Under dark condition, the higher onset bias, where the dark current of the DSSC is raised, implies better suppression of charge recombination and thereby higher V_{OC} for the DSSC.^{9, 46} The onset bias of the cells shows the trend of **DCE2** > **DCE3** > **DCE4** ≈ **DCE1**, indicating a great consistency between the results read from the V_{OC} values (under 1 sun) and dark currents (under dark) of the pertinent DSSCs. In **Figure S6a**, the IPCE spectra (400 to 800 nm) of the cells show their absorption edge decreasing as **DCE2** ≈ **DCE3** > **DCE4** ≈ **DCE1**, which agrees well with absorption spectra of the **DCE** dyes-adsorbed TiO₂ films. With the highest J_{SC} , IPCE, and V_{OC} values, the cell of **DCE2** exhibits the highest η of 8.82%, which is higher than that of N719-based cell (η = 8.68%, **Figure S6b**).

2.4. Electrochemical impedance spectra analysis

Electrochemical impedance spectra (EIS) analysis is used to investigate the impedance properties at the photoanode/electrolyte interface in the iodide-based DSSC (**Table S2**).^{47, 48} Under dark condition with an applied voltage of −0.70 V, the values of charge recombination resistance (R_{rec} , **Figure 3c**) and electron recombination lifetime (τ_e^{dark} , **Figure 3d**) decrease in an order of **DCE2** (26.55 Ω , 11.65 ms) > **DCE3** (22.49 Ω , 6.74 ms) > **DCE4** (19.09 Ω , 5.13 ms) > **DCE1** (18.70 Ω , 5.13 ms). The results provide further support of the previous conclusions: (1) double-anchored dyes indeed have better recombination retardation abilities than that of the mono-anchored dye; (2)

the retardation ability of the substituent at the phenothiazine entity of **DCE** dyes decreases in the order of 12-crown-4-substituted phenyl moiety > 4-hexoxyphenyl moiety > phenyl moiety. Under 1 sun illumination (100 mW cm^{−2}) with an open-circuit condition, charge transfer resistance (R_{ct} , **Figure S7a**) increase in the order of **DCE2** ≈ **DCE3** < **DCE4** < **DCE1**, which agrees well with their J_{SC} values. The values of τ_e^{light} (**Figure S7b**) also agree with the τ_e^{dark} values. In addition, it is notable that the values of V_{OC} , dark currents, R_{rec} , τ_e^{dark} , and τ_e^{light} , irrespective of their different measurement techniques, show a perfect consistency with one another.

2.5. Highly efficient DCE2-based DSSC with the cobalt-based electrolyte and the novel Pt-free counter electrode

When the best **DCE2**-based DSSC is performed in a cobalt-based electrolyte (**Figure 4**), a higher η of 9.52% is obtained with a much higher V_{OC} of 856.8 mV, a lower J_{SC} of 15.41 mA cm^{−2}, and a better FF of 0.72 (**Table 2**), compared to the cell parameters measured in iodide-based electrolyte. The higher V_{OC} (~150 mV higher) and lower J_{SC} for cobalt-based electrolyte are attributed to the more positive redox potential and the mass transfer limit of cobalt complex, respectively.⁴⁹

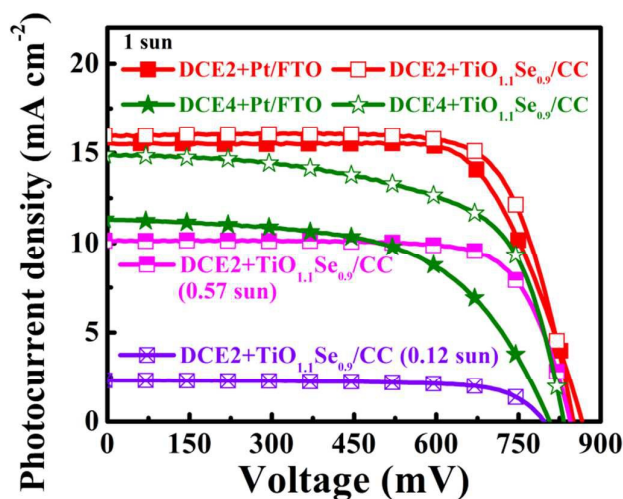


Figure 4. Photocurrent density–voltage curves of the DSSCs with **DCE2** and **DCE4** dyes, measured in a cobalt-based electrolyte using the counter electrodes of platinum/FTO and TiO_{1.1}Se_{0.9}/carbon cloth at different incident light intensities.

Table 2. Photovoltaic parameters of the cobalt-based DSSCs with **DCE2** and **DCE4** dyes^[a]

Dye	Light intensity [mW cm ^{−2}]	V_{OC} [mV]	J_{SC} [mA cm ^{−2}]	FF	η [%]	Counter electrode
DCE2	100 (1.00 sun)	856.8±7.21	15.41±0.12	0.72±0.01	9.52±0.08	Pt/FTO ^[b]
	100 (1.00 sun)	848.3±2.89	15.96±0.01	0.75±0.00	10.12±0.02	TiO _{1.1} Se _{0.9} /CC ^[c]
	57 (0.57 sun)	840.0±0.00	10.14±0.01	0.75±0.00	11.05±0.04	TiO _{1.1} Se _{0.9} /CC ^[c]
	12 (0.12 sun)	795.0±0.00	2.32±0.01	0.73±0.00	11.17±0.03	TiO _{1.1} Se _{0.9} /CC ^[c]
DCE4	100 (1.00 sun)	805.0±0.00	11.26±0.09	0.57±0.01	5.17±0.09	Pt/FTO ^[b]
	100 (1.00 sun)	830.0±0.00	14.83±0.09	0.63±0.00	7.81±0.06	TiO _{1.1} Se _{0.9} /CC ^[c]

^[a]Based on five DSSCs with tris(1,10-phenanthroline)cobalt^(II/III) trifluoromethanesulfonamide salts (Co-phen²⁺/Co-phen³⁺). ^[b]A platinum (Pt) film coated on a fluorine-doped tin oxide (FTO) conducting glass substrate. ^[c]A titanium oxide-selenide (TiO_{1.1}Se_{0.9}) ternary composite film coated on a flexible carbon cloth (CC) conducting substrate.

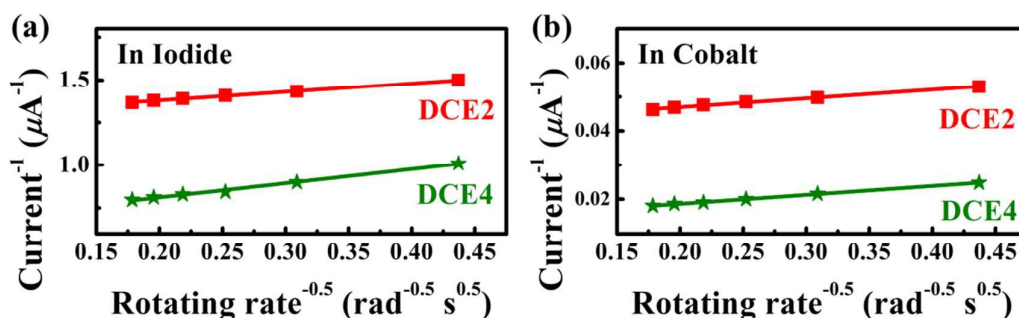
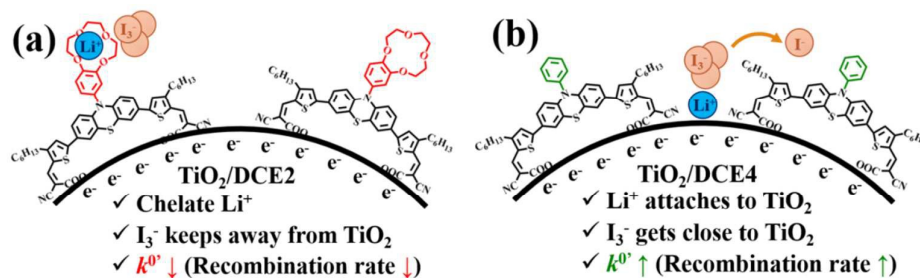


Figure 5. Plots of i^{-1} vs. $\omega^{-0.5}$ for the films of $\text{TiO}_2/\text{DCE2}$ and $\text{TiO}_2/\text{DCE4}$, measured in the (a) iodide-based and (b) cobalt-based electrolytes.



Scheme 2. The sketches of the I_3^- reduction behaviors at (a) $\text{TiO}_2/\text{DCE2}$ /electrolyte and (b) $\text{TiO}_2/\text{DCE4}$ /electrolyte interfaces.

Compared to the **DCE4**-based DSSC (5.17%), the **DCE2**-based DSSC gives a much higher η ; there is no doubt that the 12-crown-4 substituent in **DCE2** also effectively suppresses the recombination reaction in the cobalt-based electrolyte. In addition, Pt-free counter electrodes are economical alternative components of DSSCs application and attract considerable interests in recent years.⁵⁰⁻⁵² Hence, a newly designed Pt-free and TCO-free counter electrode, *i.e.*, a titanium oxide-selenide ($\text{TiO}_{1.1}\text{Se}_{0.9}$) ternary composite film coated on a flexible carbon cloth (CC) conducting substrate (denoted as $\text{TiO}_{1.1}\text{Se}_{0.9}/\text{CC}$) was synthesized. With this new counter electrode, the **DCE2**-based DSSC reaches 10.12% at 1 sun (100 mW cm^{-2}), and this cell efficiency is even higher than that obtained using traditional counter electrode of Pt/FTO. Similarly, the **DCE4**-based DSSC has better performance using $\text{TiO}_{1.1}\text{Se}_{0.9}/\text{CC}$ (7.81%) than that using Pt/FTO (5.17%). The new $\text{TiO}_{1.1}\text{Se}_{0.9}/\text{CC}$ electrode is certainly a great substitution for the traditional Pt/FTO electrode; the detailed information about $\text{TiO}_{1.1}\text{Se}_{0.9}/\text{CC}$ electrode will be published elsewhere. Last but not least, at dim light illumination, the best **DCE2**-based DSSC renders 11.05% at 0.57 sun and 11.17% at 0.12 sun in the cobalt-based electrolyte using the new $\text{TiO}_{1.1}\text{Se}_{0.9}/\text{CC}$ counter electrode (Table 2), indicating the infinite potential of this DSSC for indoor applications.

2.6. Rotating disk electrode analysis for charge recombination rate constant at the TiO_2/DCE /electrolyte interface

To explore the effect of 12-crown-4 moiety on the electron transfer at the photoanode/electrolyte interface, films of $\text{TiO}_2/\text{DCE2}$ (with crown ether) and $\text{TiO}_2/\text{DCE4}$ (without crown ether) were subjected to electrochemical studies using

rotating disk electrode (RDE) technique. Here, RDE analysis aims to simultaneously measure two key parameters, the intrinsic heterogeneous rate constant (k^0) and the effective active area (A_e), for the reduction of the oxidized redox species. When scanning from positive to negative potential at a certain rotating rate (ω), more and more negative charges (or current, i) accumulate at the TiO_2/DCE dye/electrolyte interface to trigger the reduction of the oxidized redox species. According to the simplified Koutecký–Levich equation⁵³ (Experimental Section), plots of i^{-1} vs. $\omega^{-0.5}$ were used to calculate values of k^0 and A_e , measured in an electrolyte solely containing the oxidized redox species (I_3^- for Figure 5a or Co-phen³⁺ for Figure 5b). In the iodide-based electrolyte, based on the same slope (*i.e.*, same A_e of 0.02 cm^2), the $\text{TiO}_2/\text{DCE2}$ film exhibits lower k^0 of $2.93 \times 10^{-4} \text{ cm s}^{-1}$ than the $\text{TiO}_2/\text{DCE4}$ film ($k^0 = 9.45 \times 10^{-4} \text{ cm s}^{-1}$), indicating a slower recombination rate of I_3^- ion with the accumulated negative charges at the $\text{TiO}_2/\text{DCE2}$ /electrolyte interface. It is most likely that chelation of Li^+ by **DCE2** dye at its 12-crown-4-substituted phenyl moiety, which traps I_3^- apart from the dye-uncovered TiO_2 surface due to electrostatic interaction between Li^+ and I_3^- , and thus leads to slower recombination rate (Scheme 2). In contrast, for the cobalt-based electrolyte, the more sterically congested 12-crown-4-substituted phenyl moiety (with or without Li^+ -chelation) in **DCE2** may deter the bulky oxidized redox species from getting close to the TiO_2 surface. Based on the same measured A_e of 0.54 cm^2 , $\text{TiO}_2/\text{DCE2}$ film also possesses a much lower k^0 ($4.60 \times 10^{-4} \text{ cm s}^{-1}$) than the k^0 ($14.17 \times 10^{-4} \text{ cm s}^{-1}$) of $\text{TiO}_2/\text{DCE4}$ film. Apparently, 12-crown-4 moiety-containing **DCE2** more effectively restrains the recombination reactions in both iodide-based and cobalt-based electrolytes.

Conclusions

The introduction of the 12-crown-4-substituted phenyl entity into phenothiazine-based dye with double anchors is a promising approach to reduce the charge recombination for I_3^- reduction due to Li^+ -chelation or Co-phen $^{3+}$ reduction due to steric barrier effect, at the photoanode/electrolyte interface, *i.e.*, to suppress the dark current in a DSSC. In addition to dark current measurements and electrochemical impedance spectra analyses, better dark current suppression was confirmed by rotating disk electrode technique for the first time. The best iodide-based DSSC with **DCE2** reaches an efficiency of 8.82%, which is higher than that with **DCE4** by ~21% and is also higher than that of N719-based cell. In a cobalt-based electrolyte, highest cell efficiencies of 10.12% and 11.17% are obtained at 1 and 0.12 sun, respectively.

Experimental Section

DSSCs' fabrication. A home-made transparent TiO_2 paste and a home-made scattering TiO_2 paste was prepared according to the published procedures⁵⁴. For the iodide-based electrolyte, a 20 μm -thick TiO_2 film, containing a 15 μm -thick transparent layer (Solarnix transparent paste) and a 5 μm -thick scattering layer (home-made scattering paste), was used. For the cobalt-based electrolyte, a 12 μm -thick TiO_2 film, containing an 8 μm -thick transparent layer (home-made transparent paste) and a 4 μm -thick scattering layer (another home-made scattering paste), was prepared via the same procedure. The detailed information for the TiO_2 films was depicted in the Supporting Information. The sintered TiO_2 film was immersed in 3×10^{-4} M dye solution with 10 mM of chenodeoxycholic acid (CDCA) at room temperature for at least 12 h using a mixed solvent of acetonitrile/*tert*-butanol (ACN/TBA=1:1, in volume ratio). Finally, a dye-adsorbed TiO_2 film was assembled with a sputtered-platinum/FTO counter electrode using a 25 μm -thick Surlyn[®] (SX1170-25, Solaronix S. A., Switzerland) as the cell spacer. The iodide-based electrolyte, containing 0.1 M lithium iodide (LiI), 1.0 M 1,2-dimethyl-3-propylimidazolium iodide (DMPII), 0.04 M iodine (I_2), and 0.5 M 4-*tert*-butylpyridine (TBP) in acetonitrile/3-methoxypropionitrile (ACN/MPN = 8:2, in volume ratio), was injected into the cell gap between these two electrodes by capillarity. Similarly, the cobalt-based electrolyte, containing 0.35 M tris(1,10-phenanthroline)cobalt bis(trifluoro-methanesulfonimide), 0.05 M tris(1,10-phenanthroline)cobalt tris(trifluoromethanesulfonimide), 0.8 M TBP, and 0.1 M lithium perchlorate ($LiClO_4$) in acetonitrile, was used.

Rotating disk electrode (RDE) analysis. The RDE analysis was performed in a three-electrode electrochemical system using a glassy carbon electrode (GCE, with a geometric area of 0.2 cm^2) coated with TiO_2 /**DCE2** or TiO_2 /**DCE4** film as the working electrode. The films of TiO_2 /**DCE2** or TiO_2 /**DCE4** was coated on the GCE via the drop-coating process using a precursor solution (10 μL), which contained 10 wt% of TiO_2 nanoparticle (P25), 3×10^{-4} M of DCE dye, and 10 mM of CDCA in a mixing

solvent of acetonitrile/Nafion[®] 117 solution (9/1, in volume ratio). Here, the Nafion[®] 117 solution worked as a film-forming agent to make the films coating on their GCE substrates. The loading amount of TiO_2 /**DCE2** or TiO_2 /**DCE4** film on GCE was about 0.1 mg. The obtained films of TiO_2 /**DCE2** and TiO_2 /**DCE4** were dried at 70 °C before use.

At a certain rotating speed (50, 100, 150, 200, 250, or 300 rpm), a linear sweep voltammetry (LSV) curve for the TiO_2 /**DCE2** or TiO_2 /**DCE4** film is scanned from 0.2 V to -0.3 V; in other word, more and more negative electrons accumulate at the TiO_2 /**DCE**/electrolyte interface to trigger the reduction of the oxidized redox species (I_3^- or Co-phen $^{3+}$). Thus, six LSV curves were obtained at different rotating speeds to get six values of the reciprocal currents (i^{-1}) at the formal potential (E^0) of I_3^- (**Figure S8a** and **Figure S8b**) or Co-phen $^{2+}$ /Co-phen $^{3+}$ (**Figure S8c** and **Figure S8d**). As shown in **Figure S8**, the background current signal of the GCE substrate is in an order 10^{-8} A, which can be considered to have negligible effect toward the signals of TiO_2 /**DCE** films.⁵⁵ In accordance with the simplified Koutecký-Levich equation below,⁵³ the values of k^0 and A_e can be obtained via the plots of plots of i^{-1} vs. $\omega^{-0.5}$.

$$\frac{1}{i} = \frac{1}{nFA_e k^0 C} + \frac{1}{0.62nFA_e D^{2/3} \nu^{-1/6} \omega^{1/2} C}$$

where i is the specific current obtained from the LSV curve at the formal potential of the redox mediator (I_3^- or Co-phen $^{2+}$ /Co-phen $^{3+}$), n is the number of electrons transferred, F is Faraday constant, C is the concentration of the oxidized redox species (I_3^- or Co-phen $^{3+}$), D is the apparent diffusion coefficient of the oxidized redox species, ν is the kinetic viscosity of electrolyte, and ω is the angular velocity converted from the rotating speed.

For RDE analysis, the iodide-based electrolyte contained 1.0 mM of tetrabutylammonium triiodide (I_3^-) and 0.1 M lithium perchlorate ($LiClO_4$) in acetonitrile, and the cobalt-based electrolyte included 1.0 mM of tris(1,10-phenanthroline)cobalt tris(trifluoromethanesulfonimide) (Co-phen $^{3+}$) and 0.1 M of lithium perchlorate in acetonitrile. The formal potential of Co-phen $^{2+}$ /Co-phen $^{3+}$ and the diffusion coefficient of Co-phen $^{3+}$ were measured, respectively, by the cyclic voltammetry (**Figure S9**) and another RDE analysis (**Figure S10**) in accordance with the Levich equation.⁵³ The corresponding experimental details were depicted in the Supporting Information.

Acknowledgements

We acknowledge the Support of the Academia Sinica (AS), the Ministry of Science and Technology of Taiwan, National Taiwan University, and Instrumental Center of Institute of Chemistry, AS.

Notes and references

1. A. Kojima, K. Teshima, Y. Shirai and T. Miyasaka, *J. Am. Chem. Soc.*, 2009, **131**, 6050-6051.
2. M. He, D. Zheng, M. Wang, C. Lin and Z. Lin, *Journal of Materials Chemistry A*, 2014, **2**, 5994-6003.

ARTICLE

Journal Name

3. M. He, X. Pang, X. Liu, B. Jiang, Y. He, H. Snaith and Z. Lin, *Angew. Chem. Int. Ed.*, 2016, **55**, 4280-4284.
4. X. Zhu, *Acc. Chem. Res.*, 2016, **49**, 355-356.
5. C.-Y. Chen, M. Wang, J.-Y. Li, N. Pootrakulchote, L. Alibabaei, C. Ngoc-le, J. Decoppet, J.-H. Tsai, C. Grätzel, C.-G. Wu, S. M. Zakeeruddin and M. Grätzel, *ACS Nano*, 2009, **3**, 3103-3109.
6. S. Mathew, A. Yella, P. Gao, R. Humphry-Baker, B. F. Curchod, N. Ashari-Astani, I. Tavernelli, U. Rothlisberger, M. K. Nazeeruddin and M. Grätzel, *Nat. Chem.*, 2014, **6**, 242-247.
7. Z. Yao, H. Wu, Y. Li, J. Wang, J. Zhang, M. Zhang, Y. Guo and P. Wang, *Energy Environ. Sci.*, 2015, **8**, 3192-3197.
8. K. Kakiage, Y. Aoyama, T. Yano, K. Oya, J. Fujisawa and M. Hanaya, *Chem. Commun.*, 2015, **51**, 15894-15897.
9. A. Listorti, B. O'Regan and J. R. Durrant, *Chem. Mater.*, 2011, **23**, 3381-3399.
10. M. Grätzel, *Inorg. Chem.*, 2005, **44**, 6841-6851.
11. Y. Ren, Y. Li, S. Chen, J. Liu, J. Zhang and P. Wang, *Energy Environ. Sci.*, 2016, **9**, 1390-1399.
12. J.-S. Ni, Y.-C. Yen and J. T. Lin, *Journal of Materials Chemistry A*, 2016, **4**, 6553-6560.
13. K. D. Seo, I. T. Choi and H. K. Kim, *Org. Electron.*, 2015, **25**, 1-5.
14. H. Wu, L. Yang, Y. Li, M. Zhang, J. Zhang, Y. Guo and P. Wang, *Journal of Materials Chemistry A*, 2016, **4**, 519-528.
15. J. Liu, J. Zhang, M. Xu, D. Zhou, X. Jing and P. Wang, *Energy Environ. Sci.*, 2011, **4**, 3021-3029.
16. C. H. Siu, L. T. L. Lee, P. Y. Ho, P. Majumdar, C. L. Ho, T. Chen, J. Zhao, H. Li and W. Y. Wong, *Journal of Materials Chemistry C*, 2014, **2**, 7086-7095.
17. A. Abbotto, N. Manfredi, C. Marini, F. De Angelis, E. Mosconi, J. H. Yum, Z. Xianxi, M. K. Nazeeruddin and M. Grätzel, *Energy Environ. Sci.*, 2009, **2**, 1094-1101.
18. W.-I. Hung, Y.-Y. Liao, C.-Y. Hsu, H.-H. Chou, T.-H. Lee, W.-S. Kao and J. T. Lin, *Chem. Asian J.*, 2014, **9**, 357-366.
19. X.-X. Dai, H.-L. Feng, Z.-S. Huang, M.-J. Wang, L. Wang, D.-B. Kuang, H. Meier and D. Cao, *Dyes Pigm.*, 2015, **114**, 47-54.
20. Y. S. Yang, H. D. Kim, J. H. Ryu, K. K. Kim, S. S. Park, K. S. Ahn and J. H. Kim, *Syn. Metals*, 2011, **161**, 850-855.
21. J. R. Jennings and Q. Wang, *J. Phys. Chem. C*, 2010, **114**, 1715-1724.
22. S. E. Koops, B. C. O'Regan, P. R. F. Barnes and J. R. Durrant, *J. Am. Chem. Soc.*, 2009, **131**, 4808-4818.
23. S. A. Haque, E. Palomares, B. M. Cho, A. N. M. Green, N. Hirata, D. R. Klug and J. R. Durrant, *J. Am. Chem. Soc.*, 2005, **127**, 3456-3462.
24. Y.-F. Lin, C.-T. Li, C.-P. Lee, Y.-A. Leu, Y. Ezhumalai, R. Vittal, M.-C. Chen, J.-J. Lin and K.-C. Ho, *ACS Appl. Mater. Interfaces*, 2016, **8**, 15267-15278.
25. R.-X. Dong, S.-Y. Shen, H.-W. Chen, C.-C. Wang, P.-T. Shih, C.-T. Liu, R. Vittal, J.-J. Lin and K.-C. Ho, *Journal of Materials Chemistry A*, 2013, **1**, 8471-8478.
26. R. Y.-Y. Lin, F.-L. Wu, C.-T. Li, P.-Y. Chen, K.-C. Ho and J. T. Lin, *ChemSusChem*, 2015, **8**, 2503-2513.
27. D. Kuang, C. Klein, H. J. Snaith, J.-E. Moser, R. Humphry-Baker, P. Comte, S. M. Zakeeruddin and M. Grätzel, *Nano Lett.*, 2006, **6**, 769-773.
28. H. Choi, B.-S. Jeong, K. Do, M. J. Ju, K. Song and J. Ko, *New J. Chem.*, 2013, **37**, 329-336.
29. H. Choi, J. Han, M.-S. Kang, K. Song and J. Ko, *Bull. Korean Chem. Soc.*, 2014, **35**, 1433-1439.
30. C. Nasr, S. Hotchandani, P. V. Kamat, S. Das, K. G. Thomas and M. V. George, *Langmuir*, 1995, **11**, 1777-1783.
31. C. W. Shi, S. Y. Dai, K. J. Wang, X. Pan, L. Guo, L. H. Hu and F. T. Kong, *Chin. J. Chem.*, 2005, **23**, 251-254.
32. K.-C. Huang, R. Vittal and K.-C. Ho, *Sol. Energy Mater. Sol. Cells*, 2010, **94**, 675-679.
33. J. E. Benedetti, M. A. de Paoli and A. F. Nogueira, *Chem. Commun.*, 2008, 1121-1123.
34. L. Liu, X. Li, J. Chen, Y. Rong, Z. Ku and H. Han, *Sci. Rep.*, 2013, **3**, 2413.
35. R. C. White, J. E. Benedetti, A. D. Gonçalves, W. Romão, B. G. Vaz, M. N. Eberlin, C. R. D. Correia, M. A. De Paoli and A. F. Nogueira, *J. Photochem. Photobiol., A*, 2011, **222**, 185-191.
36. Y. Uemura, T. N. Murakami and N. Koumura, *J. Phys. Chem. C*, 2014, **118**, 16749-16759.
37. M. Nishiyama, T. Yamamoto and Y. Koie, *Tetrahedron Lett.*, 1998, **39**, 617-620.
38. J. F. Hartwig, M. Kawatsura, I. H. S, K. H. Shaughnessy and L. M. Alcazar-Roman, *J. Org. Chem.*, 1999, **64**, 5575-5580.
39. A. Suzuki, *J. Organomet. Chem.*, 1999, **576**, 147-168.
40. W.-I. Hung, Y.-Y. Liao, T.-H. Lee, Y.-C. Ting, J.-S. Ni, W.-S. Kao, J. T. Lin, T.-C. Wei and Y.-S. Yen, *Chem. Commun.*, 2015, **51**, 2152-2155.
41. P. R. Barnes, K. Miettunen, X. Li, A. Y. Anderson, T. Bessho, M. Gratzel and B. C. O'Regan, *Adv. Mater.*, 2013, **25**, 1881-1922.
42. Z. Ning, Y. Fu and H. Tian, *Energy Environ. Sci.*, 2010, **3**, 1170-1181.
43. X. Jiang, K. M. Karlsson, E. Gabrielsson, E. M. J. Johansson, M. Quintana, M. Karlsson, L. Sun, G. Boschloo and A. Hagfeldt, *Adv. Funct. Mater.*, 2011, **21**, 2944-2952.
44. Z. Yao, M. Zhang, H. Wu, L. Yang, R. Li and P. Wang, *J. Am. Chem. Soc.*, 2015, **137**, 3799-3802.
45. Z. Yao, M. Zhang, R. Li, L. Yang, Y. Qiao and P. Wang, *Angew. Chem. Int. Ed.*, 2015, **54**, 5994-5998.
46. R. Li, D. Liu, D. Zhou, Y. Shi, Y. Wang and P. Wang, *Energy Environ. Sci.*, 2010, **3**, 1765-1772.
47. Q. Wang, S. Ito, M. Grätzel, J. Bisquert, T. Bessho and H. Imai, *J. Phys. Chem. B*, 2006, **110**, 25210-25221.
48. Q. Wang, J.-E. Moser and M. Grätzel, *J. Phys. Chem. B*, 2005, **109**, 14945-14953.
49. L.-L. Li and E. W.-G. Diau, *Chem. Soc. Rev.*, 2013, **42**, 291-304.
50. Q. Tai and X.-Z. Zhao, *Journal of Materials Chemistry A*, 2014, **2**, 13207-13218.
51. X. Xin, M. He, W. Han, J. Jung and Z. Lin, *Angew. Chem. Int. Ed.*, 2011, **50**, 11739-11742.
52. Y. Zhu, H. Guo, H. Zheng, Y.-n. Lin, C. Gao, Q. Han and M. Wu, *Nano Energy*, 2016, **21**, 1-18.
53. A. J. Bard and L. R. Faulkner, *Electrochemical Methods: Fundamentals and Applications*, John Wiley & Sons, Inc., New York, 2001.
54. C.-T. Li, C.-P. Lee, M.-S. Fan, P.-Y. Chen, R. Vittal and K.-C. Ho, *Nano Energy*, 2014, **9**, 1-14.
55. Y.-Y. Li, C.-T. Li, M.-H. Yeh, K.-C. Huang, P.-W. Chen, R. Vittal and K.-C. Ho, *Electrochim. Acta*, 2015, **179**, 211-219.

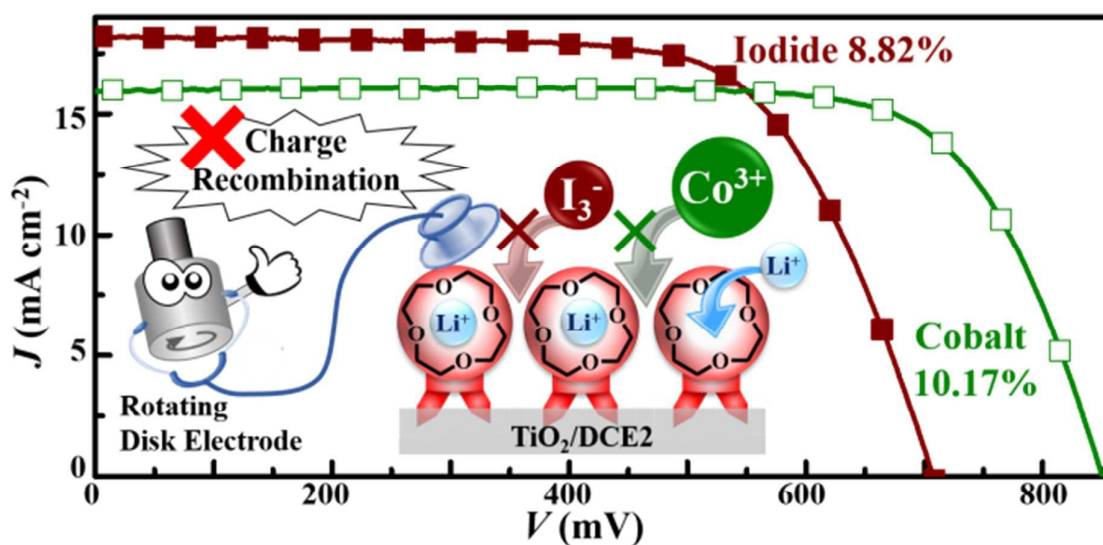
Table of Content

Effective Suppression of Interfacial Charge Recombination by 12-Crown-4 Substituent on Double-Anchored Organic Sensitizer and Rotating Disk Electrochemical Evidence

Chun-Ting Li,[†] Feng-Ling Wu,[†] Chia-Jung Liang,[†] Kuo-Chuan Ho,[‡] and Jiann T. Lin^{*,†}

[†]*Institute of Chemistry, Academia Sinica, No. 128, Sec. 2, Academia Road, Nankang District, Taipei 11529, Taiwan;* [‡]*Department of Chemical Engineering, National Taiwan University, No. 1, Sec. 4, Roosevelt Road, Taipei 10617, Taiwan*

*Corresponding authors: Tel: +886-2-2789-8522; Fax: +886-2-2783-1237; E-mail: jtlin@chem.sinica.edu.tw (Jiann T'suen Lin)



Crown-ether-substituted double-anchored organic dye surpasses the charge recombination with iodide and cobalt mediators to reach 10.12% (1 sun) and 11.17% (0.1 sun).